1.D.2 *Nuclear Physics* **A234** (1974) 185—215; © *North-Holland Publishing Co., Amsterdam*

DEFORMATIONS AND MOMENTS OF INERTIA OF ACTINIDE NUCLEI IN THE GROUND AND SHAPE ISOMERIC STATES

M. BRACK †, T. LEDERGERBER †† and H. C. PAULI †††
Institute for Theoretical Physics, Basel, Schweiz
and
A. S. JENSEN
Institute of Physics, University of Aarhus, Denmark

Received 31 May 1974

Abstract: Using a Woods-Saxon potential, equilibrium deformations are obtained by the Strutinsky shell-correction method. Deformation parameters β_2 and β_4 of the ground state and the shape isomeric state are extracted for all actinide nuclei. It is shown that the connection of β_2 and β_4 with the multipole moments Q_2 and Q_4 is not so trivial as sometimes assumed in the literature. The moments of inertia — taken at the same deformations — are evaluated within the cranking model. Their dependence on deformation and temperature (excitation energy) is discussed; the rigid body values are demonstrated to be reached both for large deformations and large temperatures. Where available, experimental data are compared; the agreement is generally very good.

1. Introduction

The experimental information on the actinide nuclei is increasing. Ground-state quadrupole and hexadecapole moments of twelve actinide nuclei were recently measured [1]). Rotational spectra built on the lowest 0^+ state of two fission isomers have been observed [2, 3]). The moments of inertia which are an indirect estimate of the deformations, are deduced. There is some hope for a more direct measurement of the quadrupole moment in the isomeric state [4]). Therefore, it seems useful to provide experimentalists with systematic tables of deformations and moments of inertia for the actinide region. Our calculations are an extension of those done by Götz *et al.* [5]), who restricted themselves to the ground states in the rare earth region.

The shell-correction approach of Strutinsky has provided an economical method to calculate deformation energy surfaces of nuclei [6, 7]). The lowest local minimum of the surface of a given nucleus is identified with its ground state, and the next higher local minimum with its (fission) isomeric state. Both these minima are stable with respect to left-right [8, 9]) and axial [10, 11]) asymmetry of the shape. Thus in this paper we restrict ourselves to axial and left-right symmetric shapes, i.e. to an elongation (c)

† Present address: Niels Bohr Institut, Blegdamsvej 17, 2100 Copenhagen, Denmark.
†† Present address: The Weizmann Institute of Science, Dept. of Nuclear Physics, Rehovot, Israel.
††† Present address: Max-Planck-Institut für Kernphysik, Heidelberg, Germany.

and a neck formation (h) parameter. For details of the shape parametrisation we refer to refs. [7, 12]).

The shell model eigenvalues, to which we apply the shell-correction method, are calculated with an average potential of the Woods-Saxon type with a constant and deformation-independent skin thickness [7, 12]). Adding these shell corrections to the liquid drop energy, whose parameters are given by Pauli and Ledergerber [13]), we obtain the total deformation energy. By minimizing this energy we find the corresponding equilibrium deformation parameters (c, h). Finally we calculate the quadrupole (Q_2) and hexadecapole moments (Q_4) of the proton and neutron density distributions of these deformations. We discuss in subsect. 2.1 the connection between the moments Q_2, Q_4 and the deformation of the potential. We show that care should be taken in relating the moments Q_2, Q_4 of the nucleon distributions to parameters β_2, β_4 extracted from the deformation of the potential.

The single-particle wave functions and energies at the two minima are furthermore used for calculating the moments of inertia by the cranking model [14]). Special interest is paid to the dependence of the moments of inertia on the pairing interaction strength and on the temperature of excited nuclei. These dependences are discussed and illustrated in subsect. 2.2.

A compilation of the results is presented in sect. 3 in the form of large tables. The results are compared to the available experimental data and a nice agreement is found.

2. Discussion of qualitative features of the nuclear moments

The shell-correction calculations with a deformed Woods-Saxon potential and the definition of the nuclear shape in terms of an elongation (c) and a neck parameter (h) have been described in detail [7, 12]) and need not be repeated here. All single-particle wave functions and energies are calculated with parameters appropriate for ^{240}Pu;

TABLE 1

Woods-Saxon parameters for ^{240}Pu (the same as quoted in ref. [12]))

	Proton		Neutron	
	central	spin-orbit	central	spin-orbit
V_0 (MeV)	−62.54	12.0	−47.46	12.0
R_0 (fm)	7.79	7.06	7.73	7.06
a (fm)	0.66	0.55	0.66	0.55

the potential energy surfaces of all other actinide nuclei are then obtained by $A^{\frac{1}{3}}$ scaling of the single-particle levels [7]). In table 1 we give the Woods-Saxon potential parameters of ^{240}Pu used in the present calculations; they are the same as in ref. [12]).

The pairing interaction is of special importance for the quantities considered here. For the moments of inertia, we use the temperature dependent BCS formalism for

which we refer to refs. [15,16]). The pairing strength G is given by [7])

$$G = \left[\tilde{g}(\lambda) \ln\left(\frac{2\Omega}{\tilde{\Delta}}\right)\right]^{-1}, \tag{1}$$

where the average level density $\tilde{g}(\lambda)$ at the Fermi energy (different for neutrons and protons) can be obtained from the energy spectrum by the Strutinsky averaging procedure [6]). The average pairing gap $\tilde{\Delta}$ and the energy interval Ω depend on the mass number A as

$$\tilde{\Delta} = \frac{c_\tau}{\sqrt{A}} \quad (\tau = \mathrm{n}, \mathrm{p}), \tag{2}$$

$$\Omega = 1.1\hbar\omega = 45\ \mathrm{MeV}/A^{\frac{1}{3}},$$

where we chose the constant $c_\tau = 12$ MeV for both neutrons and protons as in previous calculations [7]).

Since $\tilde{g}(\lambda)$ is almost independent of the nuclear deformation, through eq. (1) also the pairing strength G is essentially constant. It has been argued [17]), however, that G should be proportional to the nuclear surface area S. Such a dependence can easily be obtained in our treatment replacing $\tilde{\Delta}$ in eq. (1) by

$$\tilde{\Delta}_S = 2\Omega \left(\frac{\tilde{\Delta}_0}{2\Omega}\right)^{S_0/S}, \tag{3}$$

where $\tilde{\Delta}_0$ is given as in eq. (2) and S_0 is the surface area of the spherical nucleus.

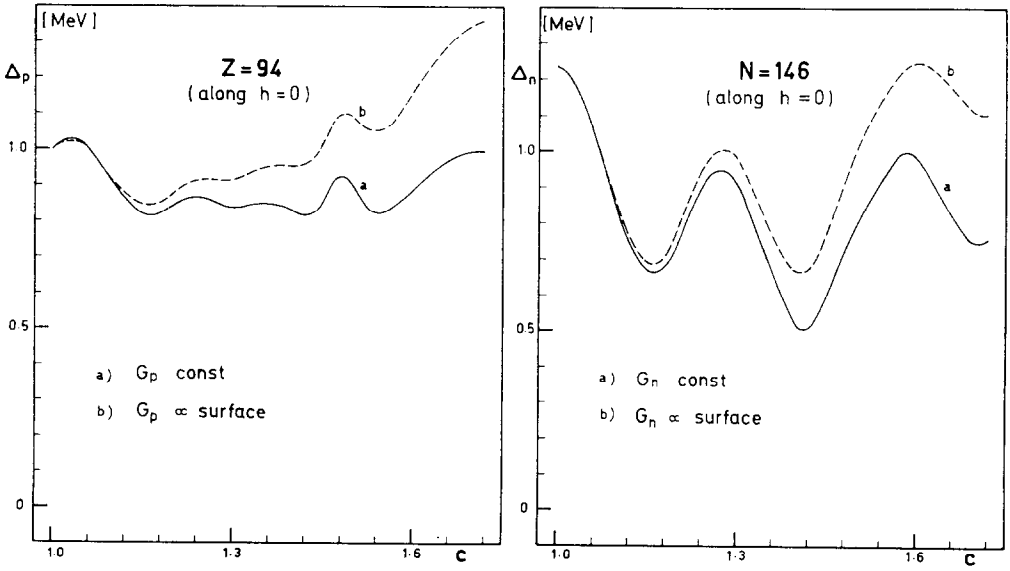

Fig. 1. Proton and neutron pairing gaps Δ_p and Δ_n as functions of the elongation parameter c. Both constant (solid lines) and surface-dependent (dashed lines) pairing strengths G are considered.

In order to demonstrate the effect of this surface dependence on the pairing gaps, we show in fig. 1 for ^{240}Pu the gaps Δ_n and Δ_p as functions of the deformation parameter c (along $h = 0$). The shell structure in the local density is clearly reflected; especially in Δ_n we see the ground-state minimum ($c \approx 1.2$) and the isomer minimum ($c \approx 1.4$). The difference between the two cases G = constant, $G \propto S$ increases with deformation. While it is negligible in the ground-state region ($c \approx 1.2$) and about 15 % at the second minimum ($c \approx 1.4$), it amounts to around 30 % at the outer fission barrier ($c \approx 1.6$). The influence of this increase on the moments of inertia will be discussed in subsect. 2.2 below.

TABLE 2

Expectation values calculated from the wave functions for some nuclei at the ground-state deformations and the second (isomeric) minima; the latter cases are marked by an asterisk

Nucleus	r_n^{rms}	r_p^{rms}	q_n	q_p	Q_2^n/N	Q_2^p/Z	Q_4^n/N	Q_4^p/Z
^{230}Th	5.85	5.69	1.22	1.25	9.7	10.3	229	278
^{232}Th	5.88	5.72	1.24	1.27	10.6	11.2	237	292
^{234}U	5.88	5.74	1.24	1.28	10.6	11.4	237	302
^{236}U	5.91	5.76	1.26	1.29	11.3	12.2	232	299
^{238}U	5.94	5.78	1.26	1.30	11.6	12.4	207	277
^{238}Pu	5.91	5.79	1.26	1.30	11.4	12.5	219	283
^{240}Pu	5.96	5.81	1.27	1.30	11.7	12.7	201	269
^{242}Pu	5.96	5.82	1.26	1.30	11.7	12.7	158	228
^{244}Pu	5.98	5.83	1.26	1.30	11.8	12.9	134	213
^{244}Cm	5.96	5.84	1.27	1.30	11.8	12.9	143	212
^{246}Cm	5.99	5.85	1.27	1.30	11.9	12.9	135	214
^{248}Cm	6.02	5.87	1.27	1.31	12.3	13.5	126	216
^{232}Th*	6.31	6.26	1.79	1.94	33.7	37.7	107	131
^{236}U*	6.38	6.34	1.81	1.97	35.2	39.2	113	133
^{236}Pu*	6.34	6.35	1.80	1.95	34.3	39.0	105	128
^{238}Pu*	6.39	6.38	1.82	1.97	35.1	40.0	112	133
^{240}Pu*	6.43	6.40	1.83	1.99	36.3	40.6	118	138
^{246}Cm*	6.53	6.51	1.86	2.04	38.5	43.2	130	153
^{254}Fm*	6.47	6.45	1.75	1.91	34.2	38.7	99	120

rms radii in fm, axis ratios q_n and q_p as defined in eq. (6), reduced quadrupole moments in fm^2 and hexadecapole moments in fm^4.

2.1. THE MULTIPOLE MOMENTS AT THE EQUILIBRIUM DEFORMATIONS

The multipole moments Q_λ and the rms radius r_{rms} of an arbitrary density distribution $\rho(r)$ are defined as

$$Q_\lambda = \sqrt{\frac{16\pi}{2\lambda+1}} \int \rho(r) r^\lambda Y_{\lambda 0}(\vartheta) \mathrm{d}\tau, \tag{4}$$

$$r_{rms} = \sqrt{\langle r^2 \rangle} = \left[\int \rho(r) r^2 \mathrm{d}\tau \Big/ \int \rho(r) \mathrm{d}\tau \right]^{\frac{1}{2}}. \tag{5}$$

We also define a generalized axis ratio q,

$$q = \left[2\int \rho(\boldsymbol{r})z^2 \mathrm{d}\tau \Big/ \int \rho(\boldsymbol{r})(x^2+y^2)\mathrm{d}\tau\right]^{\frac{1}{2}}, \tag{6}$$

where x, y, z are cartesian coordinates; in eqs. (4) and (5), $r = \sqrt{x^2+y^2+z^2}$ and ϑ is the azimuthal angle of the radius vector $\boldsymbol{r}$.

Within the independent particle model, the density $\rho(\boldsymbol{r})$ for neutrons or protons † is defined in terms of the single-particle wavefunctions $\varphi_i(\boldsymbol{r})$ as

$$\rho(\boldsymbol{r}) = 2\sum_i |\varphi_i(\boldsymbol{r})|^2 v_i^2, \tag{7}$$

where v_i^2 are the usual BCS occupation probabilities. For some selected actinide nuclei at ground-state and shape-isomeric deformations, we have calculated the above moments for protons and neutrons from the wave functions. The results are presented in table 2; the moments Q_λ are divided by the respective nucleon numbers in order to make the dependence on the deformation clearer. (The fission isomers are denoted by an asterisk.)

The nuclear radii at the ground states are known [19]) to be approximately proportional to $A^{\frac{1}{3}}$. By fitting the rms radii in table 2 with the formula

$$R_0^{(\tau)} = \sqrt{\tfrac{5}{3}\langle r_{\mathrm{rms}}^{(\tau)}\rangle^2} = r_0^{(\tau)} A^{\frac{1}{3}} \quad (\tau = \mathrm{n}, \mathrm{p}), \tag{8}$$

we find that, indeed, with the values

$$r_0^{(\mathrm{p})} = 1.20\ \mathrm{fm}, \quad r_0^{(\mathrm{n})} = 1.23\ \mathrm{fm}, \tag{9}$$

the rms radii of all ground states in table 2 are reproduced within 1 %. The agreement of the proton radius $r_0^{(\mathrm{p})} = 1.20$ fm with electron scattering data [19]) and the existence of a "neutron skin" which leads to a slightly larger radius $r_0^{(\mathrm{n})}$ are a consequence of the fact that we have used the droplet model predictions of Myers [20]) for the parameters of the Woods-Saxon potential.

Knowing the values (9) of $r_0^{(\tau)}$ which fit the rms radii eq. (5) one could expect that the reduced proton moments Q_2^{p}/Z and Q_4^{p}/Z are smaller than the corresponding neutron moments. However, the numbers in table 2 show that just the opposite is true: both reduced moments are considerably larger for protons than for the neutrons. Since the deformation of the average nuclear potential by definition is the same for protons and neutrons, this effect can only be due to the Coulomb field: it pushes the protons away from each other and enlarges the average deformation of the charge distribution. This is also reflected in the axis ratios q_τ.

This effect of the Coulomb field has to be taken into account, if one wants to relate the theoretical ground-state deformations of the average potential directly to the measured multipole moments without going over the single-particle wave functions in

† We will use indices n and p for neutrons and protons only where it is necessary.

eq. (7). Since such a procedure has been used frequently in the literature, we will discuss it here in some more detail.

In fact, one can avoid the use of the wave functions in eq. (7) in calculating the multipole moments (4), if one makes use of the approximate self-consistency of the shell model wave functions at equilibrium deformations, which means that the density distributions follow closely the average potential at these points [7, 18]). Thus one often parametrizes the density (7) by a smooth distribution $\tilde{\rho}(r)$ (e.g. of the Fermi type) with a half-density radius $R_0(\vartheta)$ which for axially and left-right symmetric deformations can be defined as

$$R(\vartheta) = R_0[1 + b_0 + \sum_{\lambda=2,4,\ldots} \beta_\lambda Y_{\lambda 0}(\vartheta)]. \tag{10}$$

The constant b_0 in eq. (10) is determined as a function of β_λ by the volume conservation condition. Assuming a constant "sharp surface" radial distribution $\tilde{\rho}(r)$, the moments $\tilde{Q}_2$ and $\tilde{Q}_4$ (for protons) are given by

$$\tilde{Q}_2 = \frac{3}{\sqrt{5\pi}} ZR_0^2\{\beta_2 + 0.360\beta_2^2 + 0.967\beta_2\beta_4 + 0.328\beta_4^2 + 0.023\beta_2^3 - 0.021\beta_2^4 + 0.499\beta_2^2\beta_4\}, \tag{11}$$

$$\tilde{Q}_4 = \frac{1}{\sqrt{\pi}} ZR_0^4\{\beta_4 + 0.725\beta_2^2 + 0.983\beta_2\beta_4 + 0.411\beta_4^2 + 0.416\beta_2^3 + 1.656\beta_2^2\beta_4 + 0.055\beta_2^4\}. \tag{12}$$

(We use here the symbols $\tilde{Q}_\lambda$ to make a distinction from the actual moments Q_λ obtained with the wave functions, i.e. with eqs. (7) and (4).) Eqs. (11) and (12) are exact up to terms of order β_2^5, β_4^3, $\beta_2^2\beta_4^2$, etc.

In the appendix, we derive the analogous formulae for $\tilde{Q}_\lambda$ for a Fermi type distribution $\tilde{\rho}(r)$. We show there, too, that the dependence of $\tilde{Q}_\lambda$ on the surface thickness a of this distribution is not unique and that one therefore can use the case $a = 0$, which leads to eqs. (11) and (12), without loosing accuracy.

In order to relate the parameters β_2 and β_4 (for $\beta_6 = \beta_8 = \ldots = 0$) with the deformation parameters c and h actually used in our calculations, we used the method presented by Pauli [12]) which up to deformations of the second minimum in the actinides agrees closely with the slightly different method used by Götz *et al.* [5]).

Instead of using different deformations for protons and neutrons, we tried to account for the Coulomb effect discussed above by renormalizing the proton radius $R_0^{(p)}$, when using eqs. (11) and (12) for the multipole moments. For the same cases as in table 2 we calculated the moments $\tilde{Q}_2$ and $\tilde{Q}_4$ with the radii

$$r_0^{(p)} = 1.27 \text{ fm}, \quad r_0^{(n)} = 1.23 \text{ fm}, \tag{13}$$

and $R_0^{(\tau)} = r_0^{(\tau)} A^{\frac{1}{3}}$. The results are shown in table 3 along with the values of β_2 and β_4 found for these cases. Comparing with the results in table 2, we see that the quadrupole moments $\tilde{Q}_2$ of the potential agree closely with the Q_2 of the actual density

distributions both for protons and neutrons. For the case of the neutrons, this result just reflects the expected approximate self-consistency of the field, which seems to hold at least for the quadrupole moments. For the protons it means that one would underestimate the quadrupole moments by about 12 % by neglecting the influence of the Coulomb field on the charge distribution.

This result is different from that of Nilsson [21]) who concluded that the quadrupole moments of the charge distributions are smaller than those of the potential, if a radius R_0 is used which approximately reproduces the rms radii. However, the difference is explained with the fact that no Coulomb potential was used in the Nilsson model of ref. [21]). We expect thus that in all calculations in which a Coulomb field is explicitly added to the average nuclear proton potential (see e.g. the recent work of Möller *et al.* [22])), the same effect should be found that the charge quadrupole moments are larger than those of the potential.

TABLE 3

Multipole moments calculated from the deformation of the potential (parameters β_2, β_4 obtained as described in the text)

Nucleus	β_2	β_4	$\bar{Q}_2^n/N$	$\bar{Q}_2^p/Z$	$\bar{Q}_4^n/N$	$\bar{Q}_4^p/Z$
^{230}Th	0.192	0.090	9.7	10.3	265	301
^{232}Th	0.208	0.087	10.5	11.2	275	312
^{234}U	0.208	0.087	10.6	11.3	278	316
^{236}U	0.224	0.078	11.4	12.2	274	311
^{238}U	0.228	0.066	11.6	12.3	249	284
^{238}Pu	0.229	0.070	11.7	12.4	261	296
^{240}Pu	0.233	0.061	11.9	12.6	244	278
^{242}Pu	0.235	0.042	11.8	12.6	199	226
^{244}Pu	0.238	0.033	11.9	12.7	179	204
^{244}Cm	0.238	0.033	11.9	12.7	180	204
^{246}Cm	0.238	0.033	12.0	12.8	181	206
^{248}Cm	0.248	0.029	12.5	13.4	182	206
^{232}Th*	0.604	0.095	35.1	37.4	106	121
^{236}U*	0.630	0.084	37.1	39.1	113	127
^{236}Pu*	0.625	0.078	36.3	38.7	108	122
^{238}Pu*	0.637	0.079	37.4	39.8	113	129
^{240}Pu*	0.646	0.082	38.1	40.7	119	135
^{246}Cm*	0.670	0.084	40.8	43.5	133	151
^{254}Fm*	0.596	0.061	35.4	37.8	101	115

The radius constants $r_0^{(\tau)}$ of eq. (13) are used. Units as in table 2.

Strictly speaking, one should also take this Coulomb effect into account in calculating the liquid drop model (LDM) part of the deformation energy. It is however not clear to which extent the surface energy would be increased by an enlarged deformation of the protons only, and therefore the balance of the surface and Coulomb energies might shift the equilibrium deformation in either direction. We expect, though, that this shift would be small in the region of nuclei considered in this paper, since the LDM energy is quite flat here and the equilibrium shapes are mainly deter-

mined by the shell-correction part of the total energy. In any case, such a change would affect both the equilibrium parameters β_2 *and* the charge quadrupole moments Q_2, and our conclusions drawn about their relation would essentially remain the same.

The hexadecapole moments $\tilde{Q}_4$ in table 3 do not reproduce the exact values of table 2 as well as the quadrupole moments; especially the neutron moments are off in some cases by more than 40 %. Thus the self-consistency argument is not valid for the hexadecapole moments. For the protons, the discrepancy between $\tilde{Q}_4$ and Q_4 is however not larger than $\approx 8\,\%$, which, in view of the numerical error discussed below, is still a sufficient accuracy.

We should finally point out that, in addition to the above discussed errors which are inherent in the single-particle model used, some numerical errors may occur in the extraction of the equilibrium deformations due to the graphical interpolation of the potential energy surfaces [7,12]). For the values of β_2, these errors are not larger than $\approx 2\,\%$; the β_4 values are, however, less accurate due to the softness of the energy surfaces in the β_4 direction [12]). Thus the absolute error in β_4 is estimated to be ± 0.005 at the ground states and ± 0.01 at the isomeric states. Regarding the partially small values of β_4, this may imply rather large relative errors in some cases.

In view of these numerical uncertainties in the values of β_2 and β_4, we can thus conclude that one may use the relations (11) and (12) together with the radii constants (13) to calculate the charge multipole moments directly from the equilibrium deformations of the potential. In detailed comparisons with the experiment, however, it might be wise to calculate the moments from the actual proton distributions, as is done in sect. 3 below.

2.2. MOMENTS OF INERTIA

Using the single-particle energies ε_i and wave functions $\varphi_i(\boldsymbol{r})$ at a given deformation, the moments of inertia can be calculated within the cranking model [14]). In the temperature-dependent BCS formalism the moments of inertia $\mathscr{J}_\parallel$ and $\mathscr{J}_\perp$ for rotation around the symmetry (z-) axis and around an axis perpendicular to it, are given by Grin [23]) (see also ref. [7])) as

$$\mathscr{J}_\parallel = \frac{\hbar^2}{2T}\sum_i \frac{\Omega_i^2}{\cosh^2(E_i/2T)}, \tag{14a}$$

$$\mathscr{J}_\perp = \hbar^2 \sum_{i,k} \left\{ \frac{(u_i v_k - u_k v_i)^2}{E_i + E_k} \left[\mathrm{tgh}\left(\frac{E_i}{2T}\right) + \mathrm{tgh}\left(\frac{E_k}{2T}\right) \right] + \frac{(u_i u_k + v_i v_k)^2}{E_i - E_k} \left[\mathrm{tgh}\left(\frac{E_i}{2T}\right) - \mathrm{tgh}\left(\frac{E_k}{2T}\right) \right] \right\} |\langle i|j_x|k\rangle|^2. \tag{14b}$$

In these equations, E_i are the quasi-particle energies and u_i, v_i the BCS occupation numbers, while j_x is the x-component of the angular momentum operator and Ω_i the eigenvalue of its z-component j_z (which commutes with the single-particle Hamilto-

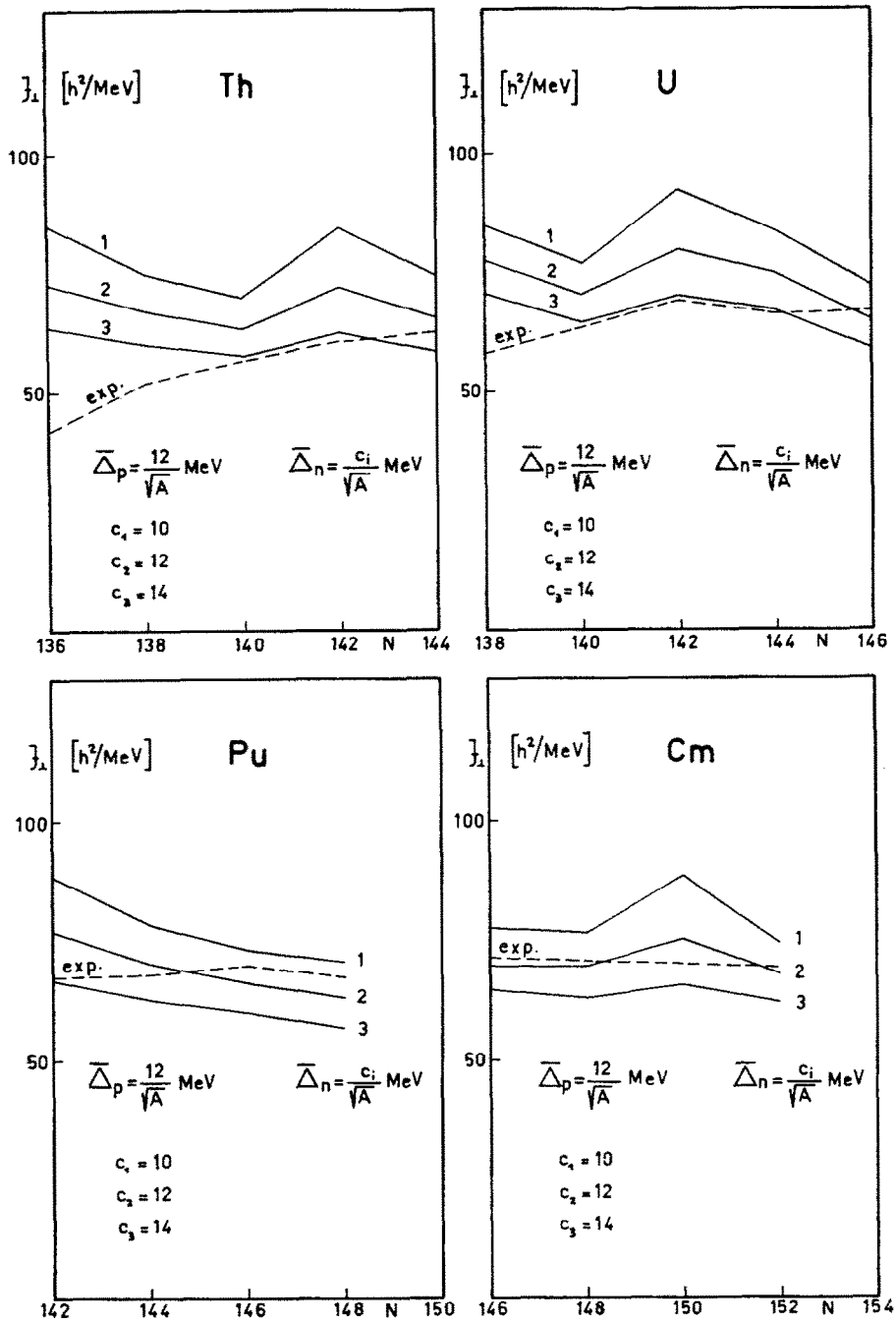

Fig. 2. Moments of inertia $\mathcal{J}_\perp$ at $T = 0$ as functions of neutron number for different isotopes. The neutron pairing strength is varied through c_n in eq. (2). The dashed curve is drawn through experimental points.

nian) in the ith state. In the limit $T = 0$, the parallel moment disappears, i.e. $\mathscr{J}_{\parallel} = 0$. Also, the second term of the perpendicular moment $\mathscr{J}_{\perp}$ vanishes in this limit, while the first term of $\mathscr{J}_{\perp}$ reduces to the usual cranking model expression.

The pairing dependence of $\mathscr{J}_{\perp}$ at zero temperature is illustrated in fig. 2 for a series of isotopes of Th, U, Pu, and Cm. The neutron pairing strength c_n in eq. (2) is varied while $c_p = 12$ MeV is fixed. For comparison, the experimental values are shown by

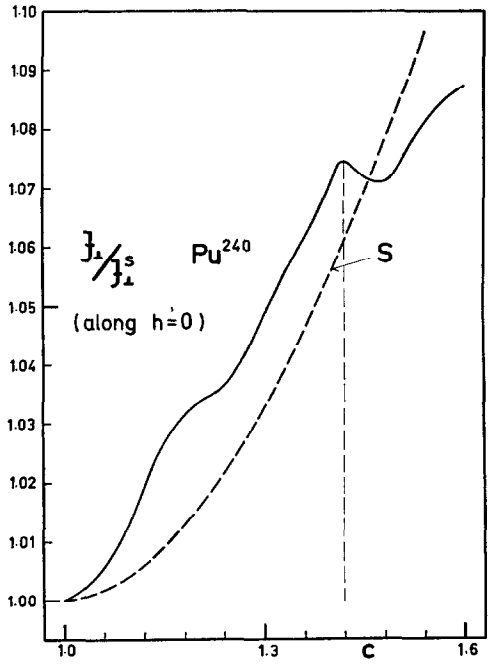

Fig. 3. The ratio $\mathscr{J}_{\perp}/\mathscr{J}_{\perp}^{S}$ of the moments of inertia for ^{240}Pu as function of deformation. Here $\mathscr{J}_{\perp}^{S}$ is evaluated with a pairing strength proportional to the surface, while $\mathscr{J}_{\perp}$ is obtained with a constant pairing strength. The dashed curve S shows the surface area of the deformed nucleus in units of that of a sphere.

the dashed lines. For the heavier isotopes a value of $c_n = 12$ MeV fits well on the average, while a larger value is favoured for lighter isotopes. An increase of c_n and c_p (and therefore of Δ_n and Δ_p) by 10 % decreases the value of $\mathscr{J}_{\perp}$ by 10–15 % for the nuclei considered here. Thus the choice of the pairing parameters is quite crucial for the moments of inertia.

Because we want to introduce as few parameters as possible we continue with the values $c_n = c_p = 12$ MeV previously used [7]). The disagreement with experiments for the lighter isotopes is not serious since deviations from the pure rotational model occur for the same nuclei (see sect. 3).

The deformation dependence of the pairing strength discussed above is therefore important for the moments of inertia. The size of the effect is shown in fig. 3. The

deformation-dependent pairing strength decreases $\mathcal{J}_\perp$ by $\approx 3\,\%$ at the ground-state deformation ($c \approx 1.2$) and by 7–8 % at a typical isomer deformation ($c \approx 1.4$). As we shall see below, this difference is not large enough to decide on the deformation dependence of pairing by using the experimental results of $\mathcal{J}_\perp$.

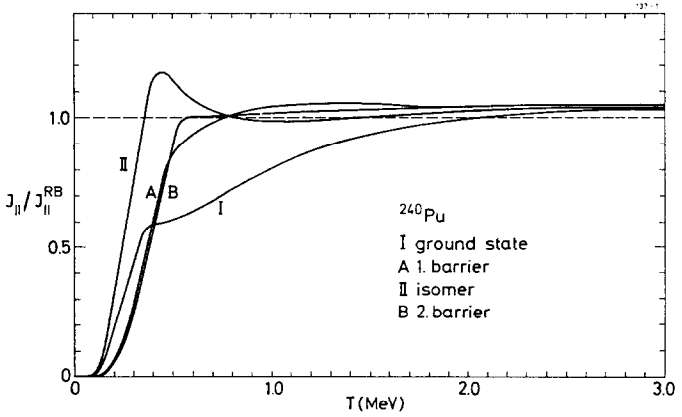

Fig. 4a. The parallel moment of inertia $\mathcal{J}_\parallel$ (in rigid body units, see eq. (15a)) as function of the temperature T. Typical deformations of ^{240}Pu are chosen.

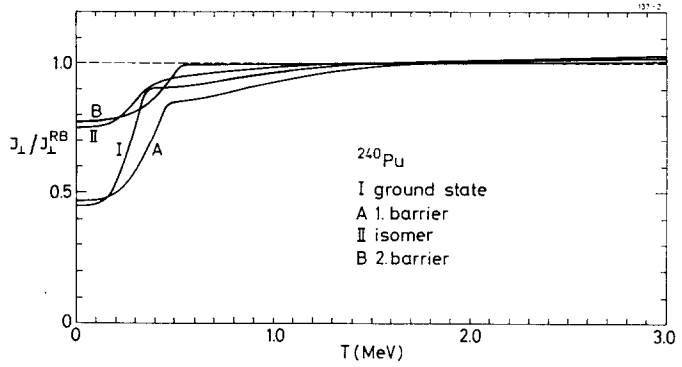

Fig. 4b. The same as fig. 4a for the perpendicular moment of inertia, $\mathcal{J}_\perp$.

It has been argued [24, 26]) that for a system of independent particles in a deformed well, the moments of inertia should approach their rigid body values in the limit of large nucleon numbers. The latter are defined by

$$\mathcal{J}_\parallel^{RB} = \int \rho(\boldsymbol{r})(x^2 + y^2)\mathrm{d}\tau, \tag{15a}$$

$$\mathcal{J}_\perp^{RB} = \int \rho(\boldsymbol{r})(x^2 + z^2)\mathrm{d}\tau, \tag{15b}$$

where $\rho(r)$ is given by eq. (7). "Large nucleon numbers" can here be substituted by [18]) "nuclei without shell structure". Once this is realized, the behaviour of $\mathscr{J}_{\parallel}$ and $\mathscr{J}_{\perp}$ discussed in the following can easily be understood.

For a few typical deformations of ^{240}Pu, $\mathscr{J}_{\parallel}/\mathscr{J}_{\parallel}^{RB}$ and $\mathscr{J}_{\perp}/\mathscr{J}_{\perp}^{RB}$ are plotted in figs. 4a and 4b as functions of the temperature T. Asymptotic values are reached for $T \gtrapprox 2$ MeV when the shell effects have disappeared. In spite of the strong deformation dependence, these limits are within 2–3 % equal to the rigid body values of eqs. (15). The sharp increase in the region $T \approx 0.2$–0.5 MeV is due to the disappearance of the gaps in this interval. As soon as $\Delta_n = \Delta_p = 0$, we have a system of independent particles still containing some shell structure. Above the critical temperature $T \approx 0.5$ MeV, the rigid body value is essentially reached, except for the small deformations (see curves I and A) for which a higher temperature is needed to wash out the shell effects [16, 18]).

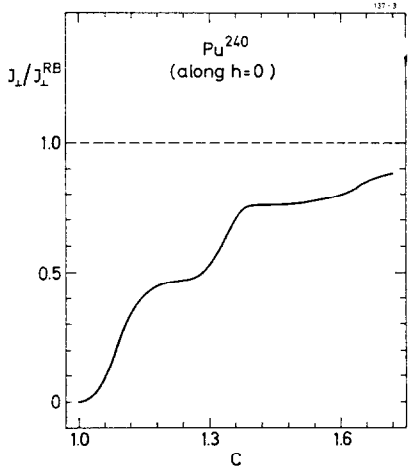

Fig. 5. The perpendicular moment of inertia (in rigid body units) as a function of deformation c.

The rigid body value of $\mathscr{J}_{\perp}$ is also reached at zero temperature in the limit of large deformations. This is demonstrated in fig. 5, where $\mathscr{J}_{\perp}$ for ^{240}Pu is plotted as a function of the elongation parameter c. The shell structure at small deformations is clearly seen. The bumps around the deformations of the two minima ($c \approx 1.2$ and 1.4) are due to the low level density leading to small pairing gaps which because of the approximate inverse proportionality in turn produce large $\mathscr{J}_{\perp}$ values. At large deformations, the rigid body value is approached although the pairing correlation still is present. This indicates that a nucleus without shell structure has a rigid body moment of inertia; the important assumption is not that the system consists of independent particles.

Since quantum mechanically a rotation around the symmetry axis is not possible, the discussion above does not hold for the parallel moment $\mathscr{J}_{\parallel}$ at $T = 0$.

TABLE 4

Ground-state deformations and moments of inertia $\mathcal{J}_\perp$ (for rotation around an axis perpendicular to the symmetry axis) for nuclei with proton and mass number Z and A

Z	A	c	h	β_2	β_4	$\mathcal{J}_\perp \left[\frac{\hbar^2}{\text{MeV}}\right]$
82	208	1.015	−0.075	−0.003	0.020	0
	210	1.015	−0.060	0.003	0.016	0
	212	1.010	−0.040	0.002	0.010	0
	214	1.000	0.000	0.000	0.000	0
	216	1.000	0.000	0.000	0.000	0
	218	1.000	0.000	0.000	0.000	0
	220	1.000	0.000	0.000	0.000	0
	222	1.180	−0.195	0.162	0.068	42
	224	1.190	−0.170	0.189	0.063	48
	226	1.195	−0.150	0.208	0.058	50
	228	1.185	−0.100	0.229	0.042	51
	230	1.180	−0.070	0.242	0.032	54
	232	1.180	−0.045	0.258	0.024	63
	234	1.155	0.000	0.250	0.007	54
	236	1.125	0.070	0.242	−0.019	49
	238	1.125	0.070	0.242	−0.019	46
	240	1.120	0.075	0.236	−0.021	44
	242	1.115	0.080	0.231	−0.023	43
84	210	1.020	−0.075	0.005	0.020	1
	212	1.015	−0.060	0.003	0.016	1
	214	1.017	−0.052	0.009	0.013	2
	216	1.020	−0.045	0.016	0.011	2
	218	1.020	−0.037	0.019	0.009	2
	220	1.120	−0.187	0.094	0.057	23
	222	1.170	−0.220	0.135	0.074	38
	224	1.185	−0.210	0.158	0.073	42
	226	1.195	−0.180	0.189	0.066	50
	228	1.200	−0.150	0.214	0.059	53
	230	1.195	−0.120	0.228	0.049	52
	232	1.180	−0.075	0.238	0.033	54
	234	1.175	−0.045	0.251	0.024	61
	236	1.165	−0.015	0.256	0.013	56
	238	1.145	0.055	0.267	−0.012	53
	240	1.130	0.060	0.245	−0.015	46
	242	1.120	0.075	0.236	−0.021	44
	244	1.115	0.080	0.231	−0.023	43
86	212	1.020	−0.060	0.010	0.016	1
	214	1.020	−0.055	0.012	0.014	2
	216	1.020	−0.037	0.019	0.009	2
	218	1.020	−0.030	0.022	0.007	2
	220	1.020	−0.015	0.028	0.003	2
	222	1.180	−0.245	0.132	0.082	42
	224	1.195	−0.240	0.151	0.083	45
	226	1.205	−0.225	0.171	0.081	48
	228	1.215	−0.200	0.198	0.076	60
	230	1.220	−0.170	0.225	0.068	61

TABLE 4 (continued)

Z	A	c	h	β_2	β_4	$\mathscr{I}_\perp \left[\frac{\hbar^2}{\text{MeV}}\right]$
	232	1.205	−0.135	0.231	0.055	56
	234	1.185	−0.090	0.235	0.039	55
	236	1.180	−0.090	0.228	0.038	60
	238	1.170	−0.020	0.260	0.015	58
	240	1.160	0.008	0.263	0.005	54
	242	1.135	0.045	0.245	−0.010	46
	244	1.125	0.070	0.242	−0.019	45
	246	1.120	0.075	0.236	−0.021	45
88	214	1.020	−0.060	0.010	0.016	0
	216	1.020	−0.037	0.019	0.009	1
	218	1.020	−0.030	0.022	0.007	2
	220	1.025	−0.015	0.036	0.003	3
	222	1.175	−0.245	0.126	0.081	44
	224	1.200	−0.245	0.153	0.086	52
	226	1.225	−0.255	0.172	0.093	59
	228	1.225	−0.232	0.188	0.086	57
	230	1.225	−0.210	0.203	0.080	65
	232	1.220	−0.172	0.223	0.068	63
	234	1.215	−0.150	0.233	0.061	61
	236	1.185	−0.090	0.235	0.039	57
	238	1.180	−0.070	0.242	0.032	64
	240	1.175	−0.037	0.256	0.021	58
	242	1.165	−0.008	0.260	0.011	55
	244	1.150	0.030	0.260	−0.003	52
	246	1.130	0.060	0.245	−0.015	47
	248	1.120	0.075	0.236	−0.021	46
90	216	1.015	−0.045	0.008	0.012	0
	218	1.015	−0.037	0.011	0.009	0
	220	1.020	−0.022	0.025	0.005	1
	222	1.020	−0.008	0.030	0.001	2
	224	1.190	−0.245	0.142	0.084	51
	226	1.230	−0.270	0.167	0.098	70
	228	1.235	−0.250	0.182	0.095	66
	230	1.235	−0.240	0.192	0.090	64
	232	1.240	−0.225	0.208	0.087	73
	234	1.225	−0.180	0.224	0.072	66
	236	1.220	−0.157	0.234	0.064	62
	238	1.195	−0.112	0.234	0.047	59
	240	1.185	−0.075	0.245	0.034	66
	242	1.180	−0.040	0.262	0.023	61
	244	1.165	−0.015	0.256	0.013	55
	246	1.150	0.015	0.251	0.001	52
	248	1.135	0.040	0.242	−0.008	48
	250	1.125	0.060	0.237	−0.016	48
92	218	1.012	−0.042	0.005	0.011	0
	220	1.015	−0.030	0.014	0.007	0
	222	1.015	−0.030	0.014	0.007	0

TABLE 4 (continued)

Z	A	c	h	β_2	β_4	$\mathcal{I}_\perp \left[\frac{\hbar^2}{\text{MeV}}\right]$
	224	1.175	−0.240	0.129	0.080	42
	226	1.215	−0.262	0.157	0.093	67
	228	1.240	−0.270	0.177	0.100	79
	230	1.240	−0.255	0.187	0.096	74
	232	1.240	−0.240	0.198	0.091	72
	234	1.240	−0.225	0.208	0.087	80
	236	1.235	−0.195	0.224	0.078	75
	238	1.220	−0.165	0.228	0.066	64
	240	1.195	−0.112	0.234	0.047	61
	242	1.180	−0.070	0.242	0.032	67
	244	1.180	−0.055	0.252	0.027	61
	246	1.175	−0.030	0.261	0.019	58
	248	1.155	0.008	0.255	0.004	53
	250	1.135	0.037	0.240	−0.007	50
	252	1.125	0.055	0.234	−0.014	49
94	220	1.010	−0.045	0.000	0.012	0
	222	1.015	−0.032	0.013	0.008	0
	224	1.015	−0.015	0.019	0.003	0
	226	1.180	−0.228	0.142	0.077	44
	228	1.220	−0.247	0.172	0.090	64
	230	1.235	−0.255	0.182	0.095	74
	232	1.240	−0.240	0.198	0.091	70
	234	1.240	−0.228	0.206	0.088	69
	236	1.240	−0.210	0.219	0.083	78
	238	1.225	−0.173	0.229	0.070	70
	240	1.215	−0.150	0.233	0.061	65
	242	1.190	−0.100	0.235	0.042	63
	244	1.180	−0.075	0.238	0.033	69
	246	1.180	−0.060	0.248	0.029	63
	248	1.175	−0.045	0.251	0.024	57
	250	1.155	−0.007	0.245	0.009	53
	252	1.130	0.045	0.236	−0.011	49
	254	1.125	0.050	0.231	−0.013	50
96	222	1.015	−0.050	0.006	0.013	0
	224	1.015	−0.037	0.011	0.009	0
	226	1.120	−0.172	0.102	0.053	26
	228	1.180	−0.210	0.153	0.072	44
	230	1.205	−0.220	0.174	0.079	59
	232	1.230	−0.230	0.194	0.087	76
	234	1.230	−0.220	0.201	0.084	73
	236	1.225	−0.195	0.213	0.076	71
	238	1.225	−0.180	0.224	0.072	77
	240	1.220	−0.165	0.228	0.066	75
	242	1.205	−0.127	0.236	0.053	70
	244	1.180	−0.075	0.238	0.033	68
	246	1.180	−0.075	0.238	0.033	75
	248	1.180	−0.060	0.248	0.029	68
	250	1.180	−0.060	0.248	0.029	63

TABLE 4 (continued)

Z	A	c	h	β_2	β_4	$\mathcal{I}_\perp \left[\frac{\hbar^2}{\text{MeV}}\right]$
	252	1.155	−0.010	0.243	0.010	53
	254	1.125	0.050	0.231	−0.013	50
	256	1.125	0.060	0.237	−0.016	52
98	224	1.015	−0.045	0.008	0.012	0
	226	1.020	−0.045	0.016	0.011	0
	228	1.125	−0.165	0.112	0.052	28
	230	1.175	−0.205	0.150	0.070	41
	232	1.190	−0.185	0.180	0.067	51
	234	1.215	−0.210	0.192	0.078	64
	236	1.220	−0.195	0.207	0.075	62
	238	1.210	−0.165	0.216	0.065	62
	240	1.210	−0.157	0.222	0.062	68
	242	1.200	−0.130	0.228	0.053	66
	244	1.185	−0.100	0.229	0.042	62
	246	1.180	−0.075	0.238	0.033	64
	248	1.180	−0.065	0.245	0.030	72
	250	1.175	−0.052	0.246	0.026	63
	252	1.175	−0.037	0.256	0.021	59
	254	1.120	0.052	0.224	−0.014	50
	256	1.120	0.052	0.224	−0.014	50
	258	1.125	0.060	0.237	−0.016	53
100	226	1.020	−0.060	0.010	0.016	0
	228	1.020	−0.045	0.016	0.011	0
	230	1.120	−0.150	0.113	0.047	27
	232	1.155	−0.170	0.147	0.057	35
	234	1.183	−0.177	0.176	0.063	48
	236	1.190	−0.158	0.197	0.059	52
	238	1.195	−0.143	0.213	0.056	56
	240	1.195	−0.135	0.218	0.053	58
	242	1.190	−0.120	0.222	0.048	63
	244	1.185	−0.090	0.235	0.039	63
	246	1.180	−0.075	0.238	0.033	62
	248	1.180	−0.068	0.243	0.031	65
	250	1.180	−0.055	0.252	0.027	72
	252	1.170	−0.040	0.247	0.021	63
	254	1.145	0.015	0.243	0.001	59
	256	1.130	0.050	0.239	−0.012	55
	258	1.125	0.060	0.237	−0.016	55
	260	1.125	0.060	0.237	−0.016	56
102	228	1.020	−0.070	0.007	0.018	0
	230	1.025	−0.045	0.024	0.011	1
	232	1.120	−0.150	0.113	0.047	27
	234	1.140	−0.150	0.139	0.049	32
	236	1.175	−0.165	0.174	0.059	45
	238	1.185	−0.150	0.196	0.056	50
	240	1.185	−0.135	0.206	0.052	54
	242	1.190	−0.120	0.222	0.048	58
	244	1.185	−0.095	0.232	0.040	63

TABLE 4 (continued)

Z	A	c	h	β_2	β_4	$\mathcal{J}_\perp \left[\frac{\hbar^2}{\text{MeV}}\right]$
	246	1.180	−0.075	0.238	0.033	63
	248	1.180	−0.070	0.242	0.032	63
	250	1.180	−0.060	0.248	0.029	66
	252	1.175	−0.045	0.251	0.024	71
	254	1.150	0.008	0.247	0.004	61
	256	1.125	0.060	0.237	−0.016	60
	258	1.125	0.070	0.242	−0.019	58
	260	1.125	0.070	0.242	−0.019	58
	262	1.125	0.075	0.245	−0.021	59
104	230	1.020	−0.060	0.010	0.016	0
	232	1.025	−0.040	0.026	0.010	1
	234	1.112	−0.140	0.108	0.043	24
	236	1.125	−0.110	0.141	0.036	29
	238	1.145	−0.110	0.169	0.038	35
	240	1.175	−0.120	0.202	0.046	46
	242	1.185	−0.125	0.212	0.049	53
	244	1.185	−0.105	0.225	0.043	55
	246	1.180	−0.085	0.232	0.036	61
	248	1.180	−0.075	0.238	0.033	62
	250	1.180	−0.060	0.248	0.029	63
	252	1.175	−0.050	0.248	0.025	64
	254	1.145	0.015	0.243	0.001	65
	256	1.125	0.065	0.239	−0.018	64
	258	1.120	0.075	0.236	−0.021	61
	260	1.120	0.075	0.236	−0.021	58
	262	1.120	0.075	0.236	−0.021	58
	264	1.120	0.075	0.236	−0.021	59
106	232	1.020	−0.050	0.014	0.013	0
	234	1.025	−0.030	0.030	0.007	2
	236	1.040	−0.015	0.060	0.003	5
	238	1.120	−0.035	0.175	0.013	30
	240	1.125	−0.075	0.160	0.026	30
	242	1.155	−0.100	0.188	0.037	37
	244	1.185	−0.120	0.215	0.047	51
	246	1.185	−0.100	0.229	0.042	54
	248	1.180	−0.080	0.235	0.035	59
	250	1.175	−0.060	0.241	0.028	60
	252	1.170	−0.030	0.253	0.018	60
	254	1.140	0.030	0.244	−0.005	60
	256	1.120	0.075	0.236	−0.021	67
	258	1.120	0.075	0.236	−0.021	66
	260	1.120	0.075	0.236	−0.021	64
	262	1.120	0.075	0.236	−0.021	61
	264	1.120	0.075	0.236	−0.021	60
	266	1.120	0.075	0.236	−0.021	61

The deformation parameters c, h and β_2, β_4 are connected as described in the text. The absolute error is ± 0.004 in β_2 and ± 0.005 in β_4. The moments $\mathcal{J}_\perp$ are in units of $\hbar^2$/MeV; their absolute error is $\approx$ 2–3 units.

Nevertheless, it reaches the rigid body value at large temperatures (see fig. 4a). This is explained by the fact that the time spent in non-symmetric orbitals increases with temperature, although the heating of a nucleus does not on the average destroy its symmetry.

Instead of using the wave functions in the definition of $\rho(\boldsymbol{r})$, eq. (7), one can evaluate the rigid body moments (15) again from a smooth density distribution in a similar way as we did it above for the multipole moments. Expressing the corresponding values by the quantities defined above in eqs. (5) and (11), we obtain

$$\tilde{\mathscr{J}}_{\parallel} = \tfrac{2}{5}A\langle\widetilde{\boldsymbol{r}^2}\rangle - \tfrac{1}{3}\tilde{Q}_2, \tag{16a}$$

$$\tilde{\mathscr{J}}_{\perp} = \tfrac{2}{5}A\langle\widetilde{\boldsymbol{r}^2}\rangle + \tfrac{1}{6}\tilde{Q}_2, \tag{16b}$$

where $\langle\widetilde{\boldsymbol{r}^2}\rangle$ is the mean square radius obtained for the smooth distribution $\tilde{\rho}(\boldsymbol{r})$, too. We found that eqs. (16) with the radii (13) reproduce the actual rigid body values (15) to within 2–3 %.

3. Results and comparison with experiment

3.1. GROUND STATES

Table 4 gives the deformation parameters (c, h) and (β_2, β_4) and moments of inertia $\mathscr{J}_{\perp}(T = 0)$ for nuclei with $208 \leqq A \leqq 266$ in their ground states, thus including the transition region between lead and actinides. We note that the transition between spherical and well deformed nuclei occurs at neutron numbers $N \approx 130$. There the values of β_2 suddenly change from 0.0 to 0.2–0.3 and stay around these values for the heavier nuclei. The parameter β_4 rises to ≈ 0.1 around $N = 136$ and falls then off rather slowly.

Only a few ground-state deformations of actinide nuclei are experimentally known [1]). Although we have concluded in subsect. 2.1 that the deformation parameters (β_2, β_4) of the potential may be used to calculate the moments Q_2 and Q_4, provided that the radius R_0 in eqs. (11) and (12) is suitably chosen (eq. 13), we want to compare the experimental moments with those obtained from the wave functions (see table 2). Fig. 6a shows the quadrupole moments. The theoretical values are systematically 2–5 % larger than the experimental ones. As the error in the theoretical numbers is 2–3 % (see subsect. 2.1), the agreement is very good.

The hexadecapole moments are compared in fig. 6b. Here the agreement is not as striking as for the quadrupole moments. The systematic behaviour of the theoretical numbers is much smoother and falls off much slower with A than the experimental values. Still, for all cases except the Cm isotopes the theoretical values lie within the experimental error limits, which however are quite large and increase for the heavier nuclei. Since also the theoretical relative errors in Q_4 are largest for the Cm isotopes due to the small values of β_4 (see tables 3 and 4), the general agreement is still satisfactory.

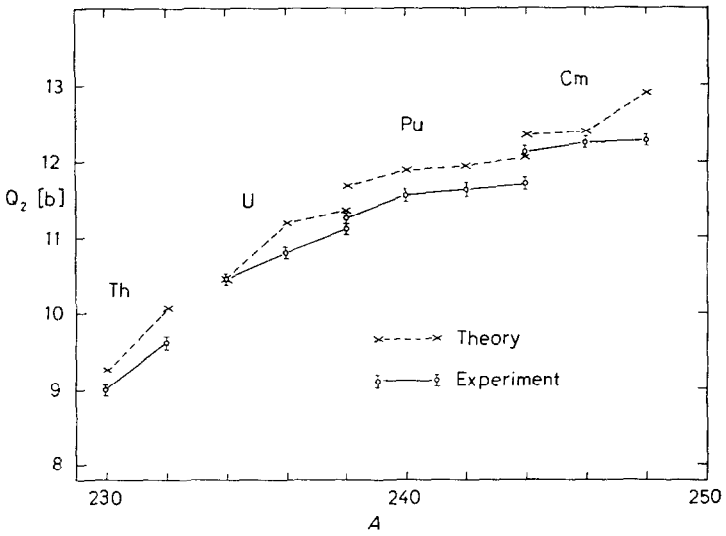

Fig. 6a. Comparison between experimental [1]) and theoretical quadrupole moments Q_2 obtained from the wave functions at the ground states.

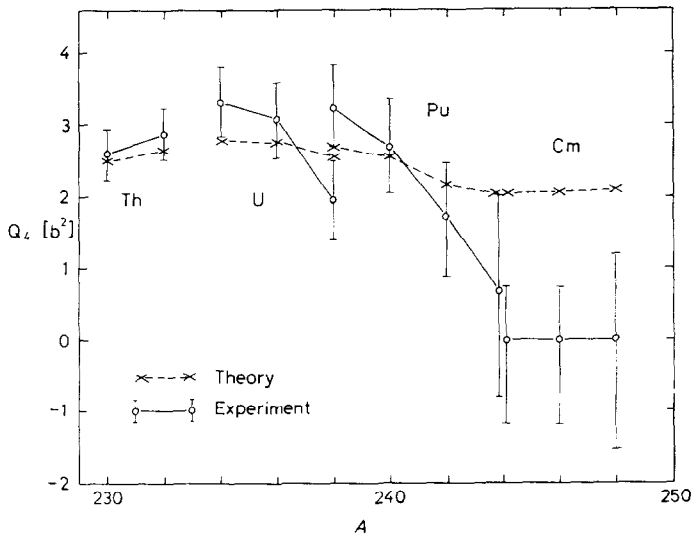

Fig. 6b. The same as fig. 6a for the hexadecapole moments, Q_4.

Very similar results have recently been obtained by Möller *et al.* [22]) using a deformed folded Yukawa potential. Their values of β_2 and β_4 (the latter ones for the case of the droplet model) agree with our values given in table 3 to within ± 0.015 (absolute values). Therefore a calculation of the quadrupole moments from the wave functions

might improve the agreement of their results with experiment (see also the discussion in subsect. 2.1).

The same quality of agreement as ours displayed in figs. 6a and 6b is also reached in recent self-consistent calculations with a density-dependent effective nucleon-nucleon interaction [27]).

TABLE 5

Comparison between experimental and theoretical moments of inertia $\mathscr{J}_\perp$

Nucleus	a (keV/$\hbar^2$)	b (eV/$\hbar^4$)	$\mathscr{J}_\perp^{\text{exp}}$ ($\hbar^2$/MeV)	$\mathscr{J}_\perp^{\text{th}}/\mathscr{J}_\perp^{\text{exp}}$
^{224}Ra	14.7	101.0	34	1.53
^{226}Ra	11.6	57.1	43	1.37
^{228}Ra	10.1	41.7	50	1.14
^{224}Th	16.1	107.0	31	1.64
^{226}Th	12.3	49.8	41	1.71
^{228}Th	9.7	18.1	52	1.27
^{230}Th	9.0	12.4	56	1.18
^{232}Th	8.4	10.7	60	1.23
^{234}Th	8.0	0.0	63	1.05
^{230}U	8.6	6.0	58	1.30
^{232}U	8.0	7.4	63	1.14
^{234}U	7.3	5.4	69	1.16
^{236}U	7.6	8.0	66	1.11
^{238}U	7.5	3.6	67	1.00
^{236}Pu	7.5	6.0	67	1.16
^{238}Pu	7.4	3.7	68	1.17
^{240}Pu	7.2	4.4	70	0.96
^{242}Pu	7.4		67	0.99
^{244}Pu	7.5		67	1.07
^{242}Cm	7.1	6.0	71	0.99
^{244}Cm	7.2	2.5	70	1.00
^{246}Cm	7.2	3.6	70	1.10
^{248}Cm	7.3	3.8	69	1.00
^{250}Cf	7.0	0.0	71	0.89
^{252}Cf	7.3		68	0.87
^{254}Fm	7.3	4.8	68	0.87

The quantities a and b are defined by eq. (17). The experimental moments of inertia are given by $\mathscr{J}_\perp^{\text{exp}} = \hbar^2/2a$, the theoretical values $\mathscr{J}_\perp^{\text{th}}$ are given in table 4. If only the 2^+ state is known experimentally, a is obtained assuming that $b = 0$ and b is omitted in the table.

The moments of inertia $\mathscr{J}_\perp$ at the ground states can be extracted from the experimental rotational spectra. These are usually parametrized by expanding the energy in powers of its total angular momentum squared,

$$E_I = aI(I+1)+bI^2(I+1)^2. \tag{17}$$

In the pure rotational model, b is zero and a is equal to $\hbar^2/2\mathscr{J}_\perp$. In table 5 we list these experimental quantities together with $\mathscr{J}_\perp$ from table 4 for all deformed doubly even nuclei whose ground-state rotational bands have been measured [28]). In fig. 7

the ratios between calculated and experimental moments are plotted. The results of two recent publications [29, 30]) utilizing the modified harmonic oscillator are also shown for comparison.

Our results deviate most strongly from the experiment in the Ra and the lighter Th isotopes. We note from table 5, however, that there is a clear correlation between these discrepancies and the b-values of the same nuclei. For those nuclei with $A < 238$, b is larger than $40\,\mathrm{eV}/\hbar^4$. This indicates that the rotational model and therefore the cranking model begin to be inappropriate for these nuclei. From table 4 we see also, that they are less deformed than the typical rotational actinides. For the

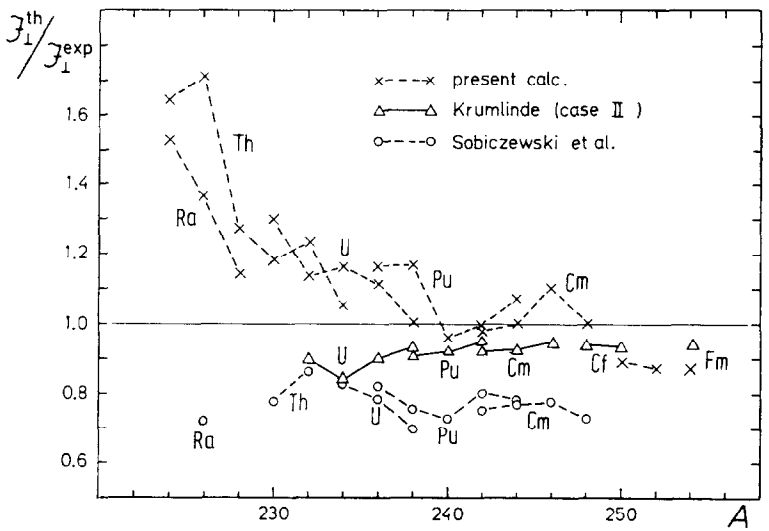

Fig. 7. Comparison between experimental and theoretical moments of inertia. The crosses are our results, circles show the calculations of ref. [30]) and triangles those of ref. [29]); in all theoretical calculations, the assumption of a constant pairing strength has been made.

rest of the nuclei, the agreement is quite satisfactory; in all cases where b is less than $10\,\mathrm{eV}/\hbar^4$, the discrepancy between our results and the experiment is less than 20 %.

On the average, our results are 5–10 % too large. This is in contrast to the results by Sobiczewski *et al.* [30]), which on the average are 15–20 % too small. With the same single-particle potential but a somewhat different treatment of the BCS pairing, Krumlinde [29]) obtained results 5–10 % too low.

The main differences in the theoretical predictions come from the choice of the pairing strength. As we have discussed in subsect. 2.2, the strong dependence of $\mathcal{J}_\perp$ on the pairing gaps would make it easy to fit the pairing parameters to obtain a better agreement. Instead, we tried to see how well we can reproduce the experiments with only one parameter. Considering this, our results are quite satisfying. In fact, the simplified treatment of the pairing effects probably makes it unreasonable to do more detailed fits of the pairing parameters. A recent investigation [31]) shows that the

TABLE 6

Isomeric-state deformations and moments of inertia, as in table 4

Z	A	c	h	β_2	β_4	$\mathcal{I}_\perp \left[\frac{\hbar^2}{\text{MeV}}\right]$
82	210	1.250	0.075	0.461	0.001	84
	212	1.255	0.075	0.470	0.002	86
	214	1.245	0.089	0.464	−0.006	85
	216	1.255	0.075	0.470	0.002	90
	218	1.260	0.080	0.483	0.001	93
	220	1.265	0.075	0.487	0.004	94
	222	1.265	0.075	0.487	0.004	93
	224	1.355	0.007	0.571	0.056	130
	226	1.365	0.000	0.580	0.061	135
	228	1.385	−0.019	0.589	0.074	134
	230	1.370	−0.004	0.583	0.064	126
	232	1.370	0.000	0.588	0.063	122
	234	1.345	0.018	0.567	0.049	115
84	210	1.260	0.058	0.464	0.009	81
	212	1.245	0.083	0.459	−0.004	84
	214	1.250	0.075	0.461	0.001	85
	216	1.255	0.089	0.482	−0.003	88
	218	1.255	0.085	0.478	−0.002	91
	220	1.245	0.105	0.477	−0.011	93
	222	1.245	0.112	0.483	−0.014	92
	224	1.270	0.080	0.501	0.004	95
	226	1.395	−0.036	0.584	0.082	138
	228	1.395	−0.036	0.584	0.082	138
	230	1.370	0.000	0.588	0.063	135
	232	1.385	−0.018	0.590	0.074	135
	234	1.385	−0.015	0.594	0.073	131
	236	1.375	−0.012	0.582	0.068	126
	238	1.370	0.000	0.588	0.063	125
86	212	1.255	0.060	0.457	0.007	80
	214	1.250	0.083	0.468	−0.002	85
	216	1.250	0.090	0.474	−0.005	86
	218	1.240	0.113	0.475	−0.016	87
	220	1.240	0.125	0.485	−0.020	91
	222	1.245	0.105	0.477	−0.011	92
	224	1.245	0.115	0.486	−0.015	93
	226	1.240	0.120	0.481	−0.018	88
	228	1.420	−0.068	0.580	0.098	164
	230	1.425	−0.056	0.603	0.098	157
	232	1.435	−0.068	0.602	0.104	155
	234	1.445	−0.075	0.606	0.110	154
	236	1.435	−0.061	0.611	0.103	150
	238	1.425	−0.050	0.611	0.097	147
	240	1.405	−0.036	0.599	0.086	136
88	214	1.255	0.064	0.460	0.006	80
	216	1.245	0.082	0.458	−0.003	83
	218	1.245	0.093	0.467	−0.007	84

TABLE 6 (continued)

Z	A	c	h	β_2	β_4	$\mathcal{J}_\perp \left[\frac{\hbar^2}{\text{MeV}}\right]$
	220	1.240	0.121	0.481	−0.019	87
	222	1.240	0.128	0.487	−0.021	90
	224	1.245	0.128	0.497	−0.020	97
	226	1.230	0.140	0.478	−0.028	90
	228	1.280	0.100	0.537	0.000	99
	230	1.425	−0.066	0.590	0.100	157
	232	1.425	−0.054	0.606	0.098	149
	234	1.440	−0.071	0.605	0.107	148
	236	1.455	−0.075	0.621	0.114	157
	238	1.460	−0.075	0.628	0.116	157
	240	1.425	−0.052	0.608	0.097	140
	242	1.415	−0.032	0.620	0.089	138
90	216	1.250	0.075	0.461	0.001	79
	218	1.245	0.095	0.469	−0.008	83
	220	1.245	0.104	0.476	−0.011	85
	222	1.235	0.136	0.484	−0.025	88
	224	1.235	0.143	0.490	−0.028	92
	226	1.235	0.150	0.496	−0.031	98
	228	1.230	0.150	0.486	−0.032	92
	230	1.220	0.164	0.478	−0.039	86
	232	1.420	−0.050	0.604	0.095	154
	234	1.420	−0.046	0.609	0.094	147
	236	1.430	−0.052	0.616	0.099	145
	238	1.435	−0.052	0.623	0.102	143
	240	1.420	−0.030	0.630	0.091	141
	242	1.415	−0.012	0.646	0.085	140
	244	1.410	−0.013	0.636	0.083	138
92	218	1.245	0.081	0.457	−0.003	80
	220	1.245	0.100	0.473	−0.010	86
	222	1.245	0.114	0.485	−0.015	88
	224	1.240	0.134	0.492	−0.024	92
	226	1.240	0.142	0.499	−0.027	96
	228	1.255	0.134	0.521	−0.020	104
	230	1.240	0.150	0.505	−0.030	98
	232	1.400	−0.014	0.619	0.079	138
	234	1.410	−0.030	0.614	0.087	143
	236	1.410	−0.018	0.630	0.084	144
	238	1.415	−0.012	0.646	0.085	150
	240	1.410	−0.011	0.639	0.082	145
	242	1.415	−0.010	0.648	0.084	143
	244	1.410	−0.006	0.646	0.081	140
	246	1.385	0.034	0.654	0.060	135
94	220	1.255	0.089	0.482	−0.003	87
	222	1.250	0.107	0.488	−0.011	92
	224	1.250	0.116	0.496	−0.014	93
	226	1.245	0.134	0.502	−0.022	97
	228	1.245	0.141	0.508	−0.025	101
	230	1.260	0.121	0.519	−0.014	107

TABLE 6 (continued)

Z	A	c	h	β_2	β_4	$\mathcal{I}_\perp \left[\frac{\hbar^2}{\text{MeV}}\right]$
	232	1.305	0.085	0.568	0.013	112
	234	1.405	−0.007	0.636	0.079	141
	236	1.400	−0.009	0.625	0.078	142
	238	1.405	−0.006	0.637	0.079	145
	240	1.410	−0.009	0.646	0.082	150
	242	1.410	−0.004	0.648	0.081	147
	244	1.415	0.000	0.662	0.082	145
	246	1.390	0.030	0.658	0.063	139
	248	1.365	0.069	0.661	0.040	137
	250	1.365	0.075	0.668	0.038	141
	252	1.365	0.093	0.689	0.032	149
	254	1.360	0.112	0.702	0.023	153
96	222	1.255	0.093	0.485	−0.005	91
	224	1.265	0.096	0.506	−0.003	99
	226	1.260	0.100	0.500	−0.006	99
	228	1.255	0.129	0.516	−0.018	103
	230	1.275	0.112	0.539	−0.006	115
	232	1.285	0.118	0.563	−0.006	118
	234	1.385	0.007	0.621	0.067	137
	236	1.405	0.000	0.645	0.077	144
	238	1.410	0.008	0.664	0.077	146
	240	1.405	−0.009	0.633	0.080	147
	242	1.410	−0.007	0.644	0.081	152
	244	1.415	0.000	0.662	0.082	151
	246	1.420	0.000	0.670	0.084	149
	248	1.385	0.041	0.663	0.057	142
	250	1.365	0.075	0.668	0.038	142
	252	1.370	0.093	0.699	0.034	151
	254	1.360	0.111	0.701	0.024	155
	256	1.360	0.120	0.712	0.020	160
98	224	1.300	0.054	0.529	0.022	98
	226	1.295	0.052	0.518	0.021	99
	228	1.275	0.098	0.526	−0.001	104
	230	1.290	0.106	0.561	0.000	115
	232	1.295	0.098	0.563	0.005	123
	234	1.330	0.075	0.603	0.025	126
	236	1.390	0.019	0.644	0.066	142
	238	1.390	0.014	0.638	0.067	144
	240	1.415	0.000	0.662	0.082	148
	242	1.410	0.000	0.653	0.080	150
	244	1.410	0.006	0.661	0.078	156
	246	1.410	0.007	0.663	0.078	152
	248	1.400	0.036	0.683	0.065	150
	250	1.370	0.075	0.677	0.040	146
	252	1.365	0.086	0.681	0.034	149
	254	1.365	0.096	0.693	0.031	154
	256	1.365	0.111	0.711	0.026	162
100	226	1.335	0.036	0.570	0.040	108

TABLE 6 (continued)

Z	A	c	h	β_2	β_4	$\mathcal{J}_\perp \left[\frac{\hbar^2}{\text{MeV}}\right]$
	228	1.330	0.052	0.579	0.033	111
	230	1.320	0.068	0.578	0.024	114
	232	1.300	0.089	0.563	0.010	117
	234	1.330	0.075	0.603	0.025	130
	236	1.370	0.044	0.640	0.050	137
	238	1.390	0.025	0.652	0.064	145
	240	1.415	0.000	0.662	0.082	151
	242	1.415	0.000	0.662	0.082	151
	244	1.415	0.000	0.662	0.082	154
	246	1.420	0.006	0.678	0.082	162
	248	1.415	0.014	0.680	0.078	158
	250	1.420	0.009	0.682	0.082	155
	252	1.380	0.038	0.650	0.056	146
	254	1.370	0.007	0.596	0.061	138
	256	1.370	0.050	0.647	0.048	150
	258	1.360	0.083	0.668	0.034	157
	260	1.370	0.075	0.677	0.040	160
102	228	1.350	0.037	0.597	0.045	115
	230	1.350	0.045	0.606	0.042	118
	232	1.345	0.057	0 611	0.036	120
	234	1.350	0.060	0.623	0.037	125
	236	1.385	0.042	0.664	0.057	138
	238	1.400	0.033	0.679	0.066	147
	240	1.405	0.027	0.680	0.070	154
	242	1.405	0.025	0.678	0.071	155
	244	1.405	0.025	0.678	0.071	155
	246	1.410	0.025	0.686	0.073	160
	248	1.412	0.025	0.690	0.074	166
	250	1.415	0.025	0.695	0.075	164
	252	1.415	0.033	0.706	0.073	162
	254	1.400	0.075	0.734	0.053	162
	256	1.385	0.080	0.712	0.045	160
	258	1.385	0.086	0.719	0.043	165
	260	1.375	0.106	0.725	0.032	170
	262	1.365	0.138	0.744	0.016	175
104	238	1.415	0.037	0.711	0.072	156
	240	1.415	0.030	0.702	0.074	159
	242	1.415	0.025	0.695	0.075	165
	244	1.415	0.022	0.691	0.076	166
	246	1.415	0.022	0.691	0.076	165
	248	1.415	0.020	0.688	0.077	168
	250	1.420	0.020	0.697	0.079	176
	252	1.420	0.020	0.697	0.079	173
	254	1.420	0.022	0.700	0.078	170
	256	1.405	0.050	0.710	0.064	167
	258	1.400	0.064	0.720	0.057	169
	260	1.400	0.070	0.727	0.055	172
	262	1.390	0.093	0.738	0.043	177
	264	1.370	0.129	0.743	0.021	186

TABLE 6 (continued)

Z	A	c	h	β_2	β_4	$\mathcal{I}_\perp \left[\frac{\hbar^2}{\text{MeV}}\right]$
106	242	1.455	0.008	0.741	0.099	171
	244	1.430	0.025	0.722	0.082	175
	246	1.420	0.020	0.697	0.079	172
	248	1.420	0.020	0.697	0.079	171
	250	1.420	0.022	0.700	0.078	175
	252	1.420	0.030	0.711	0.076	182
	254	1.420	0.030	0.711	0.076	180
	256	1.425	0.033	0.724	0.078	178
	258	1.425	0.037	0.729	0.077	177
	260	1.425	0.052	0.750	0.072	176
	262	1.425	0.055	0 754	0.071	179
	264	1.420	0.060	0.752	0.068	180
	266	1.410	0.080	0.760	0.057	182

Absolute errors ± 0.004 in β_2 and ± 0.01 in β_4 and $\approx$ 3–6 units in $\mathcal{I}_\perp$.

TABLE 7
Calculated moments for the isomeric states

Nucleus	$Q_2{}^p$	$Q_4{}^p$	$\mathcal{I}_\perp{}^{th}$	$\mathcal{I}_\perp{}^{exp}$
^{232}Th*	33.9	11.8	153	
^{236}U*	36.1	12.3	144	141
^{236}Pu*	36.7	12.0	152	
^{238}Pu*	37.6	12.5	146	
^{240}Pu*	38.2	13.0	147	150
^{246}Cm*	41.5	14.7	152	
^{254}Fm*	38.7	12.0	143	

Quadrupole moments Q_2 in b, hexadecapole moments Q_4 in b^2 and moments of inertia in $\hbar^2$/MeV. The two experimental moments of inertia [2,3]) are also given.

quadrupole components of the pairing interaction may not be neglected in calculations of moments of inertia. Also the effect of the rotation on the pairing interaction should be taken into account. This gives rise to a correction to the cranking model expression (14b), the so-called Migdal term. It is shown [31]) that this term might be comparable to the discrepancies between experiment and the simple cranking model results.

3.2. ISOMERIC STATES

For the second minima we give in table 6 the same quantities as in table 4. Very little experimental information is available so far. But recently, rotational bands built on the lowest 0^+ state were observed for ^{240}Pu [ref. [2])] and ^{236}U [ref. [3])]. Since these nuclei are almost ideal rotators in the highly deformed isomeric states, the moments of inertia can be determined and used as an indirect measurement of the

deformation of the fission isomers. The two cases, among others, are given in table 7. As we see, the theoretical values are within 2 % of the experimental ones. The Nilsson model calculations of Sobiczewski *et al.* [30]) predict values of $\mathscr{J}_\perp$ 11 % too large for ^{236}U and within 1 % for ^{240}Pu.

The surface-dependent pairing strength (see sect. 2) leads to 7–8 % (9–11 % in ref. [30])) smaller values of $\mathscr{J}_\perp$ for the fission isomers. Since our ground-state values are systematically too high, a surface independent strength seems here to give a better overall agreement with the experiment. However, the uncertainties and simplifications involved in the present treatment of the pairing make a final decision impossible at the present stage.

The quadrupole moments for the second minimum have not been measured directly yet. Serious attempts [4]) are being made, however. For the nuclei close to the most likely candidates for these experiments we calculated Q_2 and Q_4 from the wave functions at the second minimum. The results are given in table 7. Typically, as for ^{240}Pu and ^{236}U, Q_2 is 3–4 times as big as the corresponding ground-state value, i.e. 35–40 b.

4. Summary

Strutinsky's shell-correction method is used to obtain the equilibrium points of the energy surface for all actinide nuclei. The average single-particle potential applied is a deformed Woods-Saxon well of constant skin thickness; the same potential parameters and pairing strength have been used as in earlier calculations [5, 7]).

We study the relation between the multipole moments obtained either from the wave functions or from the deformation of the average potential. We see that care should be taken in relating the parameters β_2, β_4 to the moments Q_2, Q_4 of the charge distribution, because the Coulomb field appears to enlarge the deformation.

Moments of inertia are evaluated within the cranking model. Their dependence on temperature and deformation is investigated. In particular it is shown that the rigid body value is approached in the limit of both large temperatures and large (elongational) deformations.

Extensive tables of deformation parameters β_2 and β_4 and of moments of inertia $\mathscr{J}_\perp$ are given at ground states and isomeric states of actinide nuclei. Comparison with available experimental data is made. The agreement is very good, considering the fact that no parameter has been changed to improve the results. For some typical nuclei, we predict the values of Q_2 and Q_4 also at the second minimum, in the hope that the Q_2 values soon will be measured.

The authors are indebted to Prof. K. Alder and Drs. U. Götz, I. Hamamoto and Ph. Quentin for many discussions. Assistance of R. Häring with the numerical work is appreciated. Part of this work was done at the Niels Bohr Institute (M.B.), at the Weizmann Institute (T.L.) and at Nordita (A.S.J.). The hospitality and the financial support at these institutes is gratefully acknowledged.

Appendix

MULTIPOLE MOMENTS OF A FERMI DISTRIBUTION WITH FINITE SURFACE THICKNESS

We consider an axially symmetric Fermi-type density distribution

$$\rho(\boldsymbol{r}) = \frac{\rho_0}{1+\exp\left[(r-R(\vartheta))/a\right]}, \tag{A.1}$$

where the half-density radius $R(\vartheta)$ is given by

$$R(\vartheta) = R_0\{1+b_0+\beta_2 Y_2(\vartheta)+\beta_4 Y_4(\vartheta)\}. \tag{A.2}$$

The radius R_0 is constant and b_0 is a function of β_2 and β_4 determined by the volume conservation condition (see below).

Before calculating the multipole moments of the distribution (A.1), we evaluate the integral

$$I_\lambda = \int r^\lambda \rho(\boldsymbol{r}) \mathrm{d}\tau. \tag{A.3}$$

With the substitutions $x = (r-R(\vartheta))/a$ and $S = R(\vartheta)/a$ it takes the form

$$I_\lambda = \rho_0 \int \mathrm{d}\Omega R^{\lambda+2}(\vartheta) a \int_{-S}^{\infty} \frac{(1+x/S)^{\lambda+2}}{1+\mathrm{e}^x}\,\mathrm{d}x. \tag{A.4}$$

We first perform the radial integration in (A.4). One easily sees that

$$\int_{-S}^{\infty} \frac{x^{2m}}{1+\mathrm{e}^x}\mathrm{d}x = \frac{1}{2m+1} S^{2m+1} + \int_S^{\infty} \frac{x^{2m}}{1+\mathrm{e}^x}\,\mathrm{d}x \qquad (m = 0, 1, 2, \ldots),$$

$$\int_{-S}^{\infty} \frac{x^{2m-1}}{1+\mathrm{e}^x}\mathrm{d}x = \frac{-S^{2m}}{2m} + \pi^{2m}(2^{2m-1}-1)\frac{|B_{2m}|}{m} - \int_S^{\infty} \frac{x^{2m-1}}{1+\mathrm{e}^x}\,\mathrm{d}x \qquad (m = 1, 2, 3, \ldots). \tag{A.5}$$

Here we have used the definite integrals

$$\int_0^{\infty} \frac{x^{2m-1}}{1+\mathrm{e}^x}\,\mathrm{d}x = \frac{\pi^{2m}}{2m}(2^{2m-1}-1)|B_{2m}| \qquad (m = 1, 2, \ldots), \tag{A.6}$$

with the Bernoulli numbers $B_2 = \frac{1}{6}$, $B_4 = -\frac{1}{30}$, $B_6 = \frac{1}{42}$, ... Evaluating the integrals on the right hand side of (A.5), we can take advantage of the fact that in most cases of practical application, the lower limit S is much larger than unity. For a rare earth nucleus e.g., $R_0/a \approx 10$. For the nuclei and the deformations studied in this paper, we have always $R(\vartheta)/a = S > 6$. We can therefore expand and approximate them by

$$\int_S^{\infty} \frac{x^n}{1+\mathrm{e}^x}\,\mathrm{d}x \approx \int_S^{\infty} x^n \mathrm{e}^{-x}(1-\mathrm{e}^{-x}\ldots)\mathrm{d}x = n!\sum_{\nu=0}^{n} \mathrm{e}^{-S}\frac{S^\nu}{\nu!} + \mathrm{O}(\mathrm{e}^{-2S}) \qquad (S \gg 1). \tag{A.7}$$

Inserting eqs. (A.5), (A.7) into (A.4), one obtains after evaluating some algebraic sums

$$I_\lambda = \rho_0 \int \mathrm{d}\Omega \left\{ \frac{1}{\lambda+3} R^{\lambda+3}(\vartheta) + (\lambda+2)! a^{\lambda+3} \mathrm{e}^{-S} + (\pi a)^2 R^{\lambda+1}(\vartheta) \sum_{n=0}^{[\frac{1}{2}(\lambda+1)]} \binom{\lambda+2}{2n+1} \left(\frac{\pi a}{R(\vartheta)} \right)^{2n} \frac{|B_{2n+2}|}{n+1} (2^{2n+1}-1) \right\}. \quad \text{(A.8)}$$

With the diffuseness parameter d defined by

$$d = (\pi a / R_0)^2, \quad \text{(A.9)}$$

we can rewrite eq. (A.8) as

$$I_\lambda = \rho_0 \int \mathrm{d}\Omega \left\{ \frac{1}{\lambda+3} R^{\lambda+3}(\vartheta) + \frac{\lambda+2}{6} d R_0^2 R^{\lambda+1}(\vartheta) + \frac{\lambda(\lambda+1)(\lambda+2)}{6} \frac{7}{60} d^2 R_0^4 R^{\lambda-1}(\vartheta) + \ldots + \frac{(\lambda+2)!}{\pi^{\lambda+3}} d^{\frac{1}{2}(\lambda+3)} R_0^{\lambda+3} \mathrm{e}^{-S} \right\}, \quad \text{(A.10)}$$

which is exact up to terms of $\mathrm{O}(\mathrm{e}^{-2S})$. We see that for values of λ up to 4, the last term in (A.10) is always several orders of magnitude smaller than the leading terms in the region of nuclei considered here. We can therefore neglect it completely (its relative contribution to I_0 is less than 10^{-4}).

The angular integration in eq. (A.10) can now easily be performed using the orthogonality relations of the spherical harmonics in (A.2).

The volume conservation condition requires that

$$I_0 = \text{const.} = \rho_0 \tfrac{4}{3} \pi R_0^3. \quad \text{(A.11)}$$

If this is to be true independent of both deformation and diffuseness d, the value of b_0 in (A.2) has to be

$$b_0 = -\frac{1}{4\pi}(\beta_2^2 + \beta_4^2) - \tfrac{1}{3} d. \quad \text{(A.12)}$$

Eq. (A.12) is exact up to terms of order d^3, $\beta_i^2 d^2$, β_i^5, ... (Thus the terms $\propto d^2$, $\beta_i^2 d$, β_i^4 cancel identically!) The value ρ_0 of the central density is determined by setting I_0, eq. (A.11), equal to the particle number Z or N.

For the mean square radius $\tilde{R}^2$ we obtain

$$\tilde{R}^2 = I_2 = \tfrac{3}{5} Z R_0^2 \left\{ 1 + \frac{5}{4\pi}(\beta_2^2 + \beta_4^2) + \tfrac{5}{3} d + \mathrm{O}(d^2) \right\}. \quad \text{(A.13)}$$

The multipole moments $\tilde{Q}_\lambda$, defined by

$$\tilde{Q}_\lambda = \sqrt{\frac{16\pi}{2\lambda+1}} \int r^\lambda Y_{\lambda,0}(\vartheta)\rho(\boldsymbol{r})\mathrm{d}\tau, \tag{A.14}$$

can now be evaluated using the formula (A.10) with an extra factor $Y_\lambda(\vartheta)$ under the angular integration. For the first two moments we obtain (for protons)

$$\tilde{Q}_2 = \frac{3}{\sqrt{5\pi}} ZR_0^2\{\beta_2(1+\tfrac{2}{3}d)+0.360\beta_2^2+0.967\beta_2\beta_4 + 0.328\beta_4^2+0.023\beta_2^3-0.021\beta_2^4+0.499\beta_2^2\beta_4\}, \tag{A.15}$$

$$\tilde{Q}_4 = \frac{1}{\sqrt{\pi}} ZR_0^4\{\beta_4(1+3d)+(1+\tfrac{5}{3}d)(0.725\beta_2^2+0.983\beta_2\beta_4 + 0.411\beta_4^2)+0.416\beta_2^3+1.656\beta_2^2\beta_4+0.055\beta_2^4\}. \tag{A.16}$$

The first missing terms in eqs. (A.15), (A.16) are of order $d^2\beta_i$, $d^2\beta_i\beta_j$. (Note that the terms $\propto d\beta_i\beta_j$ have cancelled identically in eq. (A.15)!) Since d is ≈ 0.06 for actinide nuclei, we neglect the quadratic terms in d. The two eqs. (A.15) and (A.16) have been used in eqs. (11) and (12) for the case $d = 0$.

From these results, one might conclude that the surface thickness clearly affects the values of the multipole moments. For $d \approx 0.06$, $\tilde{Q}_2$ is increased by $\approx 4\,\%$ and $\tilde{Q}_4$ by $\approx 20\%$ compared to the value with $d = 0$. However, there is some ambiguity in this result. First, it is not clear whether the dependence on d has to be taken into account in the volume conservation condition (A.11). In the way this has been done above, $R(\vartheta)$ is for $d \neq 0$ not equal to the half-density radius, even for a spherical distribution. One might thus as well [32]) claim that $b_0 = 0$ for $\beta_i = 0$. With this, one would obtain

$$b_0 = -\frac{1}{4\pi}(\beta_2^2+\beta_4^2), \tag{A.12.1}$$

$$\tilde{R}^2 = \tfrac{3}{5}ZR_0^2\left\{1+\frac{5}{4\pi}(\beta_2^2+\beta_4^2)+\tfrac{7}{3}d+\ldots\right\}, \tag{A.13.1}$$

$$\tilde{Q}_2 = \frac{3}{\sqrt{5\pi}} ZR_0^2\{\beta_2(1+d)+0.360\beta_2^2+\ldots\}, \tag{A.15.1}$$

$$\tilde{Q}_4 = \frac{1}{\sqrt{\pi}} ZR_0^4\{\beta_4(1+4d)+(1+\tfrac{7}{3}d)(0.725\beta_2^2+\ldots)\}. \tag{A.16.1}$$

With this alternative way to conserve the volume, even the lowest-order terms in d have different factors in front.

Second, one can argue that the effective mean square radius, which is measured experimentally, depends on d. Thus, one might identify it with (following eq. (A.13))

$$\tilde{R}_{\mathrm{eff}}^2 = R_0^2(1+\tfrac{5}{3}d), \tag{A.17}$$

and express the moment in terms of it. For $\tilde{Q}_2$ e.g., one obtains then

$$\tilde{Q}_2 = \frac{3}{\sqrt{5\pi}} Z\tilde{R}_{\text{eff}}^2\{\beta_2(1-d)+0.362\beta_2^2+ \ldots\}. \qquad \text{(A.15.2)}$$

The effect of d on the moment $\tilde{Q}_4$ would then be smaller than in the case (A.16). Still another expression is obtained by doing the same with eqs. (A.13.1), (A.15.1).

We are therefore left with an ambiguity in the dependence of the moments $\tilde{Q}_\lambda$ on the diffuseness parameter d even to lowest order. This reflects that the deformation parameters β_i can be defined in different ways. They are not measurable quantities but can only be obtained indirectly through relations to the moments Q_λ. Thus the ambiguity discussed above means that they are not well defined to a percentage accuracy better than around d. Consequently, the dependence of $\tilde{Q}_\lambda$ on d is not unique and one does not lose anything using expressions like eqs. (11) and (12).

References

1) C. E. Bemis, Jr., F. K. McGowan, J. L. C. Ford, Jr., W. T. Milner, P. H. Stelson and R. L. Robinson, Phys. Rev. **C8** (1973) 1466
2) H. J. Specht, J. Weber, E. Konecny and D. Heunemann, Phys. Lett. **41B** (1972) 43
3) R. Heffner, J. Pedersen and G. Sletten, private communication (1973)
4) V. Metag, private communication (1973)
5) U. Götz, H. C. Pauli, K. Alder and K. Junker, Nucl. Phys. **A192** (1972) 1
6) V. M. Strutinsky, Nucl. Phys. **A95** (1967) 420; **A122** (1968) 1
7) M. Brack, J. Damgaard, A. S. Jensen, H. C. Pauli, V. M. Strutinsky and C. Y. Wong, Rev. Mod. Phys. **44** (1972) 320
8) P. Möller and S. G. Nilsson, Phys. Lett. **31B** (1970) 283
9) H. C. Pauli, T. Ledergerber and M. Brack, Phys. Lett. **34B** (1971) 264
10) S. E. Larsson, I. Ragnarsson and S. G. Nilsson, Phys. Lett. **38B** (1972) 269
11) U. Götz, H. C. Pauli, K. Alder and K. Junker, Phys. Lett. **38B** (1972) 274
12) H. C. Pauli, Phys. Reports **7** (1973) 35
13) H. C. Pauli and T. Ledergerber, Nucl. Phys. **A173** (1971) 398
14) D. Inglis, Phys. Rev. **96** (1954) 1059
15) P. Decowski, W. Grochulski, A. Marcinkowski, K. Siwek and Z. Wilhelmi, Nucl. Phys. **A110** (1968) 129
16) A. S. Jensen and J. Damgaard, Nucl. Phys. **A203** (1973) 578
17) S. G. Nilsson, C. F. Tsang, A. Sobiczewski, Z. Szymanski, S. Wychec, G. Gustafsson, I. L. Lamm, P. Möller and B. Nilsson, Nucl. Phys. **A131** (1969) 1
18) A. Bohr and B. Mottelson, Nuclear structure, vol. 2 (Benjamin, New York) to be published
19) L. R. B. Elton, *Introductory nuclear theory* (Pitman, London, 1959)
20) W. D. Myers, Nucl. Phys. **A145** (1970) 387
21) B. Nilsson, Nucl. Phys. **A129** (1969) 445
22) P. Möller, J. R. Nix and S. G. Nilsson, Nucl. Phys. **A229** (1974) 292
23) T. Grin, JETP (Sov. Phys.) **16** (1963) 1327
24) A. Bohr and B. Mottelson, Mat. Fys. Medd. Dan. Vid. Selsk. **30** (1955) no. 1
25) S. Belyaev, Mat. Fys. Medd. Dan. Vid. Selsk. **31** (1959) no. 11
26) G. Lüders, Z. Naturf. **15A** (1960) 371
27) Ph. Quentin, private communication (1974)
28) C. M. Lederer, J. M. Hollander and I. Perlman, *Tables of isotopes* (Wiley, New York, 1967)
29) J. Krumlinde, Nucl. Phys. **A160** (1971) 471
30) A. Sobiczewski, S. Bjørnholm and K. Pomorski, Nucl. Phys. **A202** (1973) 274
31) I. Hamamoto, Nordita preprint (1974)
32) L. W. Owen and G. R. Satchler, ORNL report 3525 (1963); Nucl. Phys. **51** (1964) 155